PHYSICAL REVIEW B **105**, 144509 (2022)

Editors' Suggestion

Robust topological superconductivity in weakly coupled nanowire-superconductor hybrid structures

Oladunjoye A. Awoga,[1,2] Jorge Cayao,[1,*] and Annica M. Black-Schaffer[1]
[1]*Department of Physics and Astronomy, Uppsala University, Box 516, 751 20 Uppsala, Sweden*
[2]*Solid State Physics and NanoLund, Lund University, Box 118, 22100 Lund, Sweden*

(Received 19 December 2021; accepted 12 April 2022; published 26 April 2022)

We investigate the role of the coupling between a spin-orbit coupled semiconductor nanowire and a conventional s-wave superconductor on the emergence of the topological superconducting phase with Majorana bound states in an applied magnetic field. We show that when the coupling is strong, the topological phase transition point is very sensitive to the size of the superconductor and in order to reach the topological phase a strong magnetic field is required, which can easily be detrimental to superconductivity. Moreover, the induced energy gap separating the Majorana bound states and other quasiparticles in the topological phase is substantially suppressed compared to the gap at zero field. In contrast, in the weak-coupling regime, we find that the situation is essentially the opposite, with the topological phase emerging at much lower magnetic fields and a sizable induced energy gap in the topological phase, which can also be controlled by the chemical potential of the superconductor. Furthermore, we show that the weak-coupling regime does not generally allow for the formation of topologically trivial zero-energy states at the wire end points, in stark contrast to the strong-coupling regime, where such states are found for a wide range of parameters. Our results thus put forward the weak-coupling regime as a promising route to mitigate the most unwanted problems present in nanowires for realizing topological superconductivity and Majorana bound states.

DOI: 10.1103/PhysRevB.105.144509

I. INTRODUCTION

The realization of Majorana bound states (MBSs) in topological superconductors (SCs) has received great attention in the last decade, not only because they represent a new state of matter but also due to their potential for novel applications [1–9]. A promising route to engineer this topological state combines one-dimensional (1D) semiconducting nanowires (NWs) with strong Rashba spin-orbit coupling (SOC), proximity-induced s-wave superconductivity, and large enough magnetic fields [10–12]. Here, MBSs emerge at the ends of the NW, and tunneling into one MBS has theoretically been shown to produce zero-bias conductance peaks with a height of $2e^2/h$ [13–15]. These ideas have motivated large experimental efforts and have already led to the fabrication of high-quality samples and zero-bias conductance measurements which, however, only partially agree with the theoretical predictions [16–23].

Part of the disagreement likely stems from the fact that recent studies have reported zero-bias conductance peaks due to topologically trivial zero-energy Andreev bound states that are therefore not related to MBSs or topology [24–55]. A particularly relevant mechanism for generating such topologically trivial zero-energy states (TZESs), very likely present in many recent experiments, is spatial inhomogeneities in the chemical potential profile [25,26,26,27,56]. Interestingly, such inhomogeneities, and thus TZESs, have been shown to naturally appear due to the finite size of the SC when strongly coupled to the NW [31,57–59]. Strong coupling between the SC and NW also leads to a renormalization of the normal-state parameters in the NW [57–67], which both substantially change the NW properties and also force the use of a larger magnetic field to reach the topological phase transition. Such large magnetic fields, in turn, can deteriorate the induced superconductivity in the NW, introducing strict requirements for the superconducting material in the strong-coupling regime. Thus, while the strong-coupling regime naturally provides a strong superconducting proximity effect in the NW, it also introduces complications that easily challenge the realization and proper identification of MBSs.

In this work we consider a 1D semiconductor NW with Rashba SOC coupled to a two-dimensional (2D) conventional s-wave SC [see Figs. 1(a) and 1(b)] and investigate the emergence of topological superconductivity at finite magnetic fields. We demonstrate that, in the weak-coupling regime, the topological phase transition does not depend on the finite size of the SC and can be reached by relatively small magnetic fields, in contrast to the strong-coupling regime, where strong dependence on SC size exists and substantially larger magnetic fields are required. Most interestingly, we find that the induced energy gap in the topological phase at weak

---

[*] Corresponding author: jorge.cayao@physics.uu.se

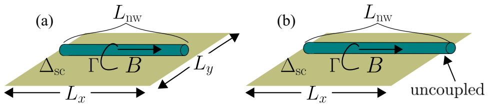

FIG. 1. (a) Schematics of a 1D NW (cyan) with length $L_{\rm nw}$ in a parallel magnetic field B coupled with strength Γ to a 2D SC with superconducting order parameter $\Delta_{\rm sc}$ and length L_x and width L_y (green). (b) Same as (a), but part of the NW is not coupled to the SC, remaining in the normal state, such that the NW-SC hybrid system forms a SN junction.

coupling is similar to or even larger than the gap in strongly coupled NWs. Moreover, this energy gap is tunable by the chemical potential in the SC, such that it easily acquires large values for both thin and thick SCs, which is crucial for the topological protection of MBSs. Furthermore, we show that TZESs do not emerge in the weak-coupling regime, contrary to the strong-coupling regime, which is plagued by the natural appearance of TZESs. Our results thus demonstrate that the weak-coupling regime of NW-SC systems is surprisingly beneficial for low magnetic field topological superconductivity and topologically protected MBSs.

The remainder of this paper is organized as follows. We introduce the model and method used in this study in Sec. II. In Sec. III we present the phase diagram of the system and discuss the effects of finite size and chemical potential of the SC on the topological phase transition. In Sec. IV we compare the induced energy gap in the topological phase for weakly and strongly coupled NW-SC systems and also illustrate the sensitivity of the induced energy gap to the chemical potential of the SC. In Sec. V, we discuss the absence or presence of TZESs from a coupling strength perspective. Finally, in Sec. VI, we present our conclusions.

II. MODEL AND METHOD

We consider a one-dimensional NW with strong SOC in a parallel magnetic field, which induces a Zeeman field B, coupled to a conventional 2D spin-singlet s-wave SC, as schematically shown in Fig. 1(a). The total coupled NW-SC system is modeled by

$$H = H_{\rm nw} + H_{\rm sc} + H_{\Gamma}, \tag{1}$$

where

$$\begin{aligned}
H_{\rm nw} &= \sum_{x,\sigma,\sigma'} d^{\dagger}_{x\sigma}\big[\varepsilon_{\rm nw}\sigma^{0}_{\sigma,\sigma'} + B\sigma^{x}_{\sigma,\sigma'}\big]d_{x\sigma'} \\
&\quad + \sum_{x,\sigma,\sigma'} d^{\dagger}_{x\sigma}\big[-t_{\rm nw}\sigma^{0}_{\sigma,\sigma'} + i\alpha_{\rm nw}\sigma^{y}_{\sigma,\sigma'}\big]d_{x+1,\sigma'} + {\rm H.c.}, \\
H_{\rm sc} &= \sum_{ij\sigma} c^{\dagger}_{i\sigma}[\varepsilon_{\rm sc}\delta_{i,j} - t_{\rm sc}\delta_{\langle i,j\rangle}]c_{j\sigma} \\
&\quad + \sum_{i} \Delta_{\rm sc}(c^{\dagger}_{i\uparrow}c^{\dagger}_{\downarrow} + c_{i\downarrow}c_{i\uparrow}), \\
H_{\Gamma} &= -\Gamma\sum_{x,i\sigma} c^{\dagger}_{i\sigma}d_{x\sigma}\delta_{i_x,x}\delta_{i_y,\frac{L_y+1}{2}} + {\rm H.c.}
\end{aligned}$$

Here, $H_{\rm nw}$ represents the 1D NW Hamiltonian, where the operator $d_{x,\sigma}$ destroys an electron with spin σ at site x in the NW of length $L_{\rm nw}$, σ^{i} is the i-Pauli matrix in spin space, $\varepsilon_{\rm nw} = (2t_{\rm nw} - \mu_{\rm nw})$ is the NW on-site energy, $\mu_{\rm nw}$ is the NW chemical potential, $t_{\rm nw}$ is the nearest-neighbor NW hopping strength, B is the Zeeman interaction that results from the external magnetic field along the NW, and $\alpha_{\rm nw}$ is the Rashba SOC hopping strength. Moreover, $H_{\rm sc}$ represents the Hamiltonian of the 2D SC with length L_x and width L_y, where $c_{i,\sigma}$ destroys an electron with spin σ at site $i = (i_x, i_y)$ in the SC, $\varepsilon_{\rm sc} = (4t_{\rm sc} - \mu_{\rm sc})$ is the on-site energy, $\delta_{\langle i,j\rangle}$ implies only nearest-neighbor hopping is allowed, and $\Delta_{\rm sc}$ is the spin-singlet s-wave (i.e., on-site) order parameter. Last, H_{Γ} denotes the coupling between the NW and SC with coupling strength $\Gamma \leqslant t_{\rm sc}$, where, as seen in Fig. 1(a), the NW is positioned to the middle of the 2D SC.

We solve the full NW-SC system in Eq. (1) within the Bogoliubov–de Gennes formalism [68] for experimentally realistic parameters. Since we are mainly interested in the low-energy states, we take advantage of the sparseness of the Hamiltonian in Eq. (1) and carry out a partial diagonalization using the Arnoldi iteration method [69] to extract the low-energy spectrum. We have further verified that self-consistent calculations of the superconducting order parameter do not modify the results presented here [59,70–72]. The parameters we consider in the SC are $t_{\rm sc} = 15$meV and $|\Delta_{\rm sc}| = 0.1t_{\rm sc}$, which is in the range of experimentally measured values for NbTiN [5]. For the NW we use $t_{\rm nw} = 4t_{\rm sc}$, which is consistent with earlier works [31,59] and accounts for the difference in the effective masses and lattice constant mismatch in the NW and SC. For the NW we also use $\mu_{\rm nw} = 0.02t_{\rm nw}$, and $\alpha_{\rm nw} = 0.05t_{\rm nw}$. The SOC strength is then $\alpha_{\rm R} = 2a\alpha_{\rm nw}$, giving $\alpha_{\rm R} = 0.9\,$eVÅ, when using a lattice constant $a = 1.5\,$nm, which is a large value but in line with reports for InSb and InAs NWs [5]. We further consider a NW of length $L_{\rm nw} = 1000a = 1.5\,\mu$m, again realistic for experiments. The length of the SC is taken to be substantially longer than the NW to avoid boundary effects from the SC, while we usually vary the width of the SC. For the setup in Fig. 1(b) the NW is left partly uncovered by the SC to simulate a superconductor-normal state (SN) junction, where we keep the N part $L_{\rm N} = 4a$ long. In what follows, all energies are given in units of $t_{\rm sc}$, and lengths are in units of the lattice constant a.

The NW-SC system, modeled by Eq. (1), is expected to enter into a topological phase, with MBSs at the ends of the NW, for Zeeman fields B above a critical value $B_{\rm c}$, namely, $B > B_{\rm c}$ (see, e.g., [4]). Here, all the ingredients, SOC, superconductivity, and a Zeeman field, are crucial to reach the topological phase. Of particular importance is the proximity-induced superconductivity in the NW, characterized by the induced energy gap $\Delta_{\rm ind}$, which is effectively determined by the lowest energy level, i.e., closest to zero, in the full NW-SC spectrum,

$$\Delta_{\rm ind} = \begin{cases} |E_0|, & B < B_{\rm c}, \\ |E_1|, & B > B_{\rm c}, \end{cases} \tag{2}$$

where $E_{0(1)}$ is the lowest (first excited) energy level. Here, the first excited energy level is needed in the topological phase, $B > B_{\rm c}$, since E_0 corresponds to the energy of the MBSs that appear at or close to zero. In order to visualize

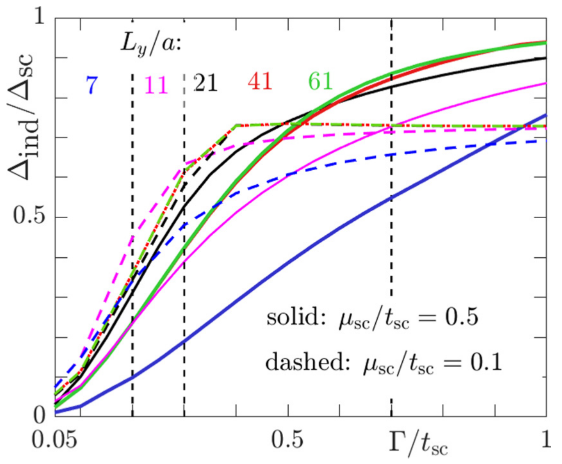

FIG. 2. Induced energy gap in the NW Δ_{ind} as a function of NW-SC coupling strength Γ for several different values of L_y and μ_{sc} at zero Zeeman field $B = 0$. Vertical dashed lines denote the weak, $\Gamma/t_{\mathrm{sc}} = 0.2, 0.3$, and strong, $\Gamma/t_{\mathrm{sc}} = 0.7$, coupling values used throughout our work and $\mu_{\mathrm{nw}}/t_{\mathrm{nw}} = 0.02$. For the remaining parameters, see the text.

the behavior of Δ_{ind}, we present in Fig. 2 the dependence of Δ_{ind} on Γ for several SC widths L_y and chemical potentials μ_{sc} at $B = 0$. We see that, although there is an appreciable sensitivity to these parameters, in general, $\Delta_{\mathrm{ind}} \propto \Gamma$ at low Γ, while Δ_{ind} has a nonlinear and saturating behavior at larger Γ. This identifies two distinct regimes: we refer to Δ_{ind} linear in Γ as the *weak-coupling regime*, while we refer to Δ_{ind} nonlinear in Γ as the *strong-coupling regime*. For our parameters the weak-coupling regime is generally present when $0 < \Gamma/t_{\mathrm{sc}} \leqslant 0.3$. We therefore probe these two different regimes by fixing $\Gamma/t_{\mathrm{sc}} = 0.2$, 0.3 for weak coupling and $\Gamma/t_{\mathrm{sc}} = 0.7$ for strong coupling (see vertical dashed lines in Fig. 2). This definition of the weak- and strong-coupling regimes is also qualitatively consistent with earlier works [64,65].

The strong-coupling regime has attracted a large amount of attention lately mainly because it allows for large induced gaps that are similar in size to those in the parent SC at $B = 0$ (see Fig. 2 and, e.g., [18,23]). However, as we discussed in the Introduction, the strong-coupling regime also brings unwanted effects such as renormalization of the normal-state NW parameters and the formation of TZESs that can easily obscure unambiguous identification of MBSs (see, e.g., [59]).

III. PHASE DIAGRAM

As explained in the previous section, the setup modeled by Eq. (1) realizes a topological phase for large enough Zeeman fields with MBSs located at the ends of the NW. To proceed, we first analyze how the phase diagram, which shows the appearance of trivial and topological phases, depends on properties of the SC, in particular L_y and μ_{sc}. To characterize the phase diagram, we calculate the topological invariant using the Wilson loop W [72–75]. For this purpose we use the setup in Fig. 1(a) and also assume that L_x and L_{NW} are infinitely long, such that the wave vector along x, k_x, is a good quantum number. Then W is obtained as [73,74]

$$\begin{aligned} W &= \det[\hat{U}_{\mathrm{o}}(-\pi)^{\dagger}\hat{U}_{\mathrm{o}}[-\pi + (n-1)\delta k_x] \\ &\quad \times \prod_{i=1}^{n-2}\{\hat{U}_{\mathrm{o}}[-\pi + (i+1)\delta k_x]^{\dagger}\hat{U}_{\mathrm{o}}(-\pi + i\delta k_x)\} \\ &\quad \times \hat{U}_{\mathrm{o}}(-\pi + i\delta k_x)^{\dagger}\hat{U}_{\mathrm{o}}(-\pi)] \\ &= e^{i\gamma}, \end{aligned} \tag{3}$$

where $W = +1$ (-1) dictates that the system is in the topologically trivial (nontrivial) phase. Here, $\hat{U}_{\mathrm{o}}$ is the matrix of occupied states and a function of k_x, δk_x is the discretization of k_x, n is the number of discretized points, and γ is the Berry phase. Note that $\hat{U}_{\mathrm{o}}(-\pi)$ is used instead of $\hat{U}_{\mathrm{o}}(\pi)$ since the wave functions are the same at the boundaries of the Brillouin zone and this trick makes W gauge invariant. The quantity W in Eq. (3) provides the same information as the Pfaffian but is simpler to calculate; see [76,77] for related Pfaffian studies.

In Fig. 3(a) we plot W as a function of B and Γ for several different values of L_y and fixed $\mu_{\mathrm{sc}}/t_{\mathrm{sc}} = 0.5$, where each curve represents the topological phase transition (TPT) separating the trivial and topological regimes. This TPT corresponds to a critical Zeeman field denoted B_{c}. The general observation is that the TPT curves exhibit a strong dependence on L_y when the SC is not in the bulk regime. When reaching the bulk regime, $L_y/a \geqslant 41$ in our case, this dependence saturates, and the TPT curves appear to be superimposed. Most importantly, each TPT curve strongly depends on the values of Γ, where larger Zeeman fields are needed to reach the topological phase when Γ is large, whereas notably lower Zeeman fields are enough at weak Γ. There is thus an interplay between the size of the SC and the coupling to the NW which strongly affects the TPT. This effect can be understood to arise from an effective energy shift induced in the NW when the coupling Γ is strong, which both renormalizes the NW chemical potential and makes it strongly dependent on L_y [59,66]. This, in turn, moves the TPT to higher B values, even possibly making it difficult to reach the topological phase without destroying superconductivity at strong coupling. In contrast, the renormalization of the chemical potential in the weak-coupling regime is negligibly small, and hence, the TPT does not depend very much on L_y in this regime. Moreover, as noted above, the weak-coupling regime requires relatively small Zeeman fields to reach the TPT for essentially all reasonable widths of the SC.

As elucidated above, the TPT separating the trivial and topological regimes is highly dependent on the coupling strength and SC thickness. Given fixed coupling and thickness, which is the realistic setup, we next explore the possibility to control the TPT by tuning the chemical potentials in the NW and SC, μ_{nw} and μ_{sc}, which are experimentally tunable by means of voltage gates. In Fig. 3(b) we present the critical Zeeman fields B_{c} needed to reach the TPT as a function of μ_{sc} in the weak, $\Gamma/t_{\mathrm{sc}} = 0.2$, 0.3, and strong, $\Gamma/t_{\mathrm{sc}} = 0.7$, coupling regimes for a fixed thin SC with $L_y/a = 11$ and $\mu_{\mathrm{nw}} = 0.02t_{\mathrm{nw}}$. Here, we focus on a thin SC, $L_y/a = 11$, motivated by the thin SCs currently employed in several experiments (see, e.g., [18,23]). For completeness, we also provide the corresponding results for a bulk SC with $L_y/a =$

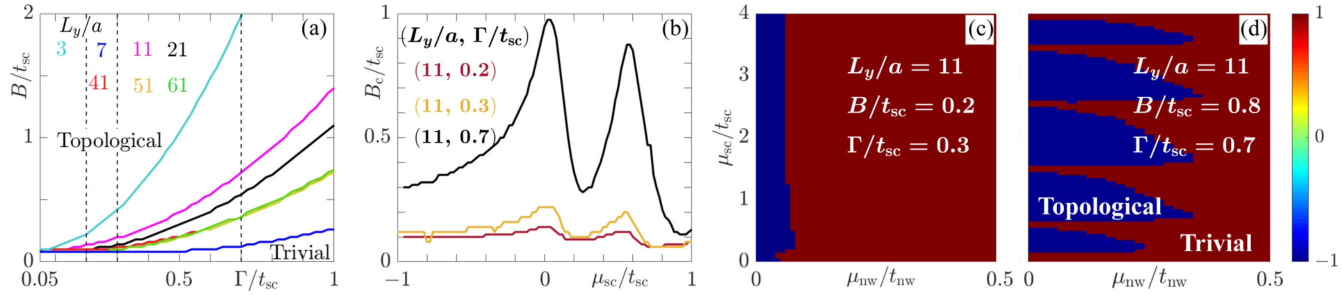

FIG. 3. (a) Topological phase diagram calculated using the Wilson loop W as a function of coupling Γ and Zeeman field B for several different SC widths using $\mu_{\rm nw}/t_{\rm nw} = 0.02$ and $\mu_{\rm sc}/t_{\rm sc} = 0.5$. The curves denote TPT, i.e., $B_{\rm c}$ for each L_y. Vertical lines denote weak (two leftmost line) and strong (rightmost line) coupling. (b) Critical field $B_{\rm c}$ as a function of $\mu_{\rm sc}$ for a thin SC, $L_y = 11a$, at weak (red and yellow) and strong (black) coupling. W as a function of $\mu_{\rm nw}$ and $\mu_{\rm sc}$ for $L_y/a = 11$ [purple curve in (a)] for (c) weak coupling and (d) strong coupling.

41 in Appendix A. We observe that the TPT in Fig. 3(b) is largely insensitive to $\mu_{\rm sc}$ at weak coupling (red and yellow) but very sensitive to it at strong coupling (black). This result is qualitatively unchanged for a bulk SC (see Appendix A). Moreover, the critical fields $B_{\rm c}$ are much larger for strong coupling compared to weak coupling, implying that $B_{\rm c}$ could even be experimentally unreachable for some values of $\mu_{\rm sc}$ as superconductivity might be destroyed before reaching $B_{\rm c}$. In stark contrast, in the weak-coupling regime, a low Zeeman field is enough for the system to reach $B_{\rm sc}$ and thus become topological, highlighting again a clear advantage for weakly coupled hybrid systems.

Having seen that the weak-coupling regime needs lower Zeeman fields to reach the topological phase, we finally present in Figs. 3(c) and 3(d) the phase diagram, calculated using W, as a function of $\mu_{\rm nw}$ and $\mu_{\rm sc}$ for $L_y/a = 11$ in the weak- and strong-coupling regimes, respectively, and for fixed, but different, B. In the weak-coupling case [Fig. 3(c)], the topological phase emerges at small NW doping and is notably largely insensitive to the SC doping. The latter is a result of the negligible renormalization of the NW chemical potential at weak coupling. For strong coupling, a substantially larger B is needed to produce a phase diagram with a reasonably sized topological region [see Fig. 3(d)], and even then there is a strong dependence on the properties of the SC. We have verified that the phase diagrams remain qualitatively the same when changing B or L_y or both.

To summarize the results above, the topological phase in strongly coupled NW-SC hybrid structures is very sensitive to the properties of the SC and notably also needs strong Zeeman fields, which can easily be detrimental to superconductivity. In stark contrast, the topological phase in the weak-coupling regime is not sensitive the properties of the SC and instead only requires that the NW is lightly doped, which opens a promising route for low Zeeman field topological superconductivity and MBSs.

IV. LOW-ENERGY SPECTRUM AND INDUCED GAP

Having established that a sizable topological phase regime emerges at low Zeeman fields in the weak-coupling regime of NW-SC hybrid structures, we next investigate the possibility to produce appreciable induced energy gaps $\Delta_{\rm ind}$, defined in Eq. (2). The need for a large induced gap in the topological phase, often simply called the topological gap, is motivated by the fact that this gap separates the discrete MBSs from the quasicontinuum, thus providing the operation protection of MBSs from quasiparticle poisoning (see, e.g., [17,78]). The induced gap is set by the proximity-induced superconductivity in the NW. As a consequence, stronger coupling between the NW and SC is expected to generate a larger energy gap. However, as we established in the previous section, strong coupling also requires larger Zeeman fields to reach the topological regime and additionally renormalizes the properties of the NW, and it is *a priori* not clear whether these might also have an effect on the topological gap. In this section, we therefore investigate the induced gap for both strong and weak coupling across the TPT and into the topological phase.

We start by obtaining the low-energy spectrum in the setup schematically shown in Fig. 1(a) with both the SC and NW considered to be finite and the NW terminated within the SC to avoid boundary effects from the SC. In Figs. 4(a)–4(c) we plot the low-energy spectrum as a function of Zeeman field B (renormalized by $B_{\rm c}$) in both the weak (red and yellow curves) and strong (black curve) coupling regimes for several different values of $\mu_{\rm sc}$. Note that only the lowest positive energy levels are shown for visualization purposes. In general, for all $\mu_{\rm sc}$ and Γ, a substantial induced energy gap is opened at $B = 0$. In this zero-field limit, the induced gap is particularly large in the strong-coupling regime, and it represents proximity-induced superconductivity in the NW with effective order parameter $\Delta_{\rm ind}$. By increasing the Zeeman field, $\Delta_{\rm ind}$ overall becomes smaller due to Zeeman depairing, and it eventually even vanishes when $B = B_{\rm c}$ (black arrows) since the bulk spectrum necessarily closes at the TPT. Beyond the TPT, the induced gap $\Delta_{\rm ind}$, the topological gap, again acquires a finite value in the topological phase, but notably, now it is the energy gap separating the MBS and the first excited state. As a side note, we have verified that the MBSs spatially reside in the NW (SC) in the weak (strong) coupling regime, thus conditioning the regions where they have to be probed; for details see Appendix B.

What is most remarkable in Figs. 4(a)–4(c) is that the topological gap is generally very similar in the weak- and strong-coupling regimes. In particular, the topological gap is not much smaller, and instead is sometimes even larger, for weak coupling compared to strong coupling. This is very different from the behavior at low Zeeman fields, where strong

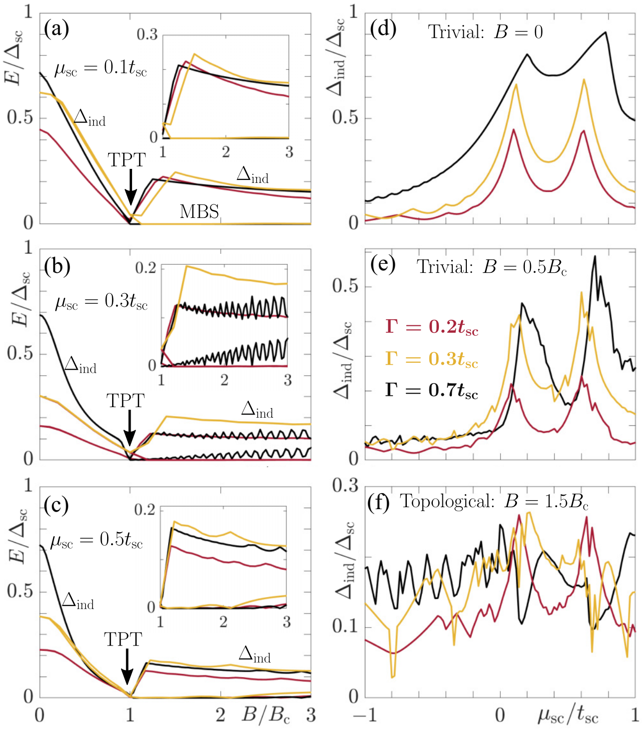

FIG. 4. (a)–(c) Low-energy spectrum as a function of the normalized Zeeman field B/B_c for weak and strong coupling Γ at different SC chemical potentials μ_{sc} for the geometry depicted in Fig. 1(a). (d)–(f) Induced gap Δ_{ind} extracted from (a)–(c) using Eq. (2) as a function of μ_{sc} for weak and strong coupling Γ at different Zeeman fields B. Here, $L_y/a = 11$, and $\mu_{nw}/t_{nw} = 0.02$.

coupling always gives the larger gap. Moreover, the topological gap also varies with μ_{sc}, which enables an experimental tunable level of control. The surprising similarity in topological gap sizes in the weak- and strong-coupling regimes can be explained by an interplay of effects. First of all, strong coupling should generate stronger induced superconductivity in the NW, which should naively give a larger induced gap compared to those of weakly coupled structures. But strong coupling also renormalizes the NW normal-state properties; in particular it reduces the SOC strength (see, e.g., [59]), and the topological gap is known to be proportional to the SOC [79]. Thus, the topological gap is directly reduced by this SOC renormalization always present in strongly coupled structures. On the other hand, at weak coupling, the SOC is not renormalized (or only slightly renormalized in the worst case), resulting in a sizable topological gap, despite the initially smaller Δ_{ind} at $B = 0$ in this regime. Moreover, strong coupling also requires a larger Zeeman field to reach the TPT, which further suppresses the induced gap compared to the weak-coupling regime. Taken together, we find that the interplay of these effects results in very similar induced gaps in the topological phase for weakly and strongly coupled NW-SC hybrid structures.

To further elucidate the behavior of the induced gap Δ_{ind}, particularly its tunability, we plot in Figs. 4(d) and 4(e) Δ_{ind} as a function of μ_{sc} for both weak and strong coupling at several different B. At $B = 0$, Δ_{ind} is substantially larger in the strong-coupling regime compared to weak coupling for all μ_{sc}, albeit hole doping does not favor the proximity effect as much and generates a smaller Δ_{ind} [see Fig. 3(d)]. As the Zeeman field increases but $B < B_c$, Δ_{ind} decreases due to the detrimental effect of magnetism on superconductivity [see Fig. 4(e)]. This suppression of Δ_{ind} is larger in the strong-coupling regime for a fixed ratio of B/B_c, as B_c is then also larger. In the topological regime, $B > B_c$, the situation is notably different from that at zero field: overall, the induced gap Δ_{ind} is similar in the weakly and strongly coupled regimes. We also observe that by tuning μ_{sc}, Δ_{ind} can easily be even larger in a weakly coupled NW-SC hybrid structure than in the strongly coupled regime. This is both a surprising and highly useful result as it implies that weakly coupled NW-SC hybrid structures can achieve a topological gap similar to or even larger than that in strongly coupled structures and that the gap is also tunable. We have verified that these findings remain robust for larger bulklike SC (see Appendix A) and also in the presence of weak to moderate scalar disorder in the superconductor (results to be published elsewhere).

In summary, weakly coupled NW-SC hybrid structures can achieve robust topological superconductivity with a large topological gap and stable MBS. In contrast, the large induced gap in the trivial phase of strongly coupled NW-SC hybrid structures does not translate into a large induced gap in the topological phase due to the combined detrimental effects of large magnetic fields and significant reduction of SOC.

V. TRIVIAL ZERO-ENERGY STATES

Hitherto we have focused on the setup in Fig. 1(a) where the whole NW is in contact with the SC. As a final part, we study the setup presented in Fig. 1(b), where part of the NW is left uncovered with the SC, thus forming an effective SN junction. This type of junction is experimentally relevant in transport experiments but has been shown to host TZESs in the strong-coupling regime, with properties similar to those of MBSs (see, e.g., [59,66]). Here we are interested in exploring whether TZESs emerge in SN junctions in weakly coupled NW-SC hybrid structures. To address this question, we plot in Fig. 5 the low-energy spectrum obtained by solving Eq. (1) for the setup in Fig. 1(b) as a function of coupling, SC chemical potential, and Zeeman field.

To start, we display in Figs. 5(a) and 5(b) the low-energy spectrum as a function of the Zeeman field for two different values of Γ. In the case of strong coupling [Fig. 5(a)], the low-energy spectrum has a finite induced gap at $B = 0$, as expected, but this gap is then reduced as B increases and also gives rise to the formation of TZESs for $B < B_c$, well before the TPT. After the TPT, the system hosts a pair of MBSs at zero energy, which exhibit spectral properties similar to those of the TZESs. The appearance of the TZES is a consequence of the renormalization of the NW chemical potential in the S part of the NW. Then, because the NW chemical potential in the uncoupled N region is left unchanged, the full NW develops an effective potential that resembles that of a quantum dot forming in the N part of the junction. This quantum dot region favors the formation of bound states, which can easily appear at zero energy. The quantum dot TZESs are also located at the wire end point, just like the topologically protected MBSs, and therefore, they become very challenging to distinguish from

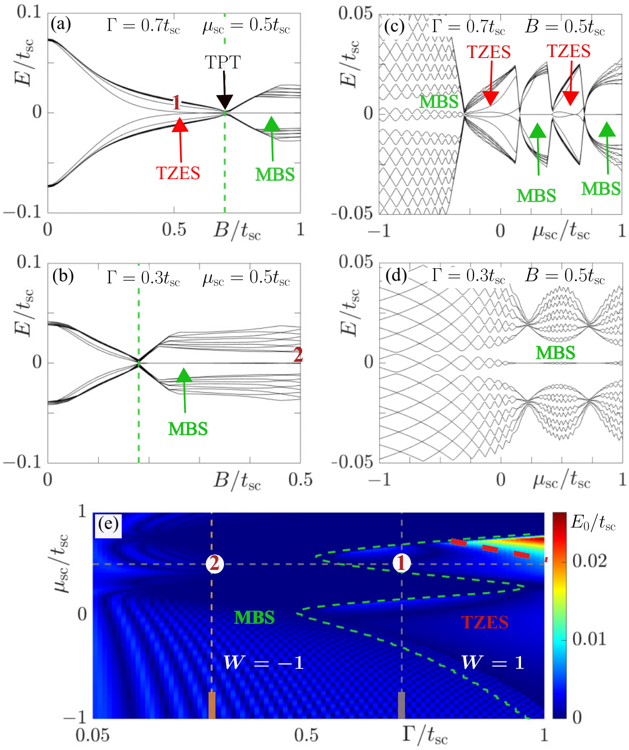

FIG. 5. Low-energy spectrum as a function of the Zeeman field B for (a) strong and (b) weak coupling Γ at fixed $\mu_{sc}/t_{sc} = 0.5$ for the geometry depicted in Fig. 1(b). Points 1 and 2 corresponds to the same points in (e). Low-energy spectrum as a function of chemical potential in the SC μ_{sc} for (c) strong and (d) weak coupling at fixed magnetic field $B/t_{sc} = 0.5$. (e) Lowest positive energy plotted in a color scale as a function of μ_{sc} and Γ for fixed $B/t_{sc} = 0.5$. Dashed vertical lines indicate weak and strong coupling, while dashed green curve denotes TPT with topological MBS to the left and TZEs to the right. The trivial phase hosts TZESs between the green (TPT) and dashed red curves. Here $L_y/a = 11$, and $\mu_{nw}/t_{nw} = 0.02$.

MBSs. In stark contrast to the strong-coupling regime, we find for the weak coupling that the SN junction does not host any TZESs below B_c, only MBSs for $B > B_c$ [see Fig. 5(b)]. Using the same argument as above, this stems from the fact that the NW chemical potential profile in the weak-coupling regime is not overly affected by the SC, thereby avoiding the creation of an unwanted quantum dot with TZESs.

The results above can be further confirmed by obtaining the low-energy spectrum as a function of the SC chemical potential in the weak- and strong-coupling regimes at a fixed magnetic field, as shown in Figs. 5(c) and 5(d). While the strong-coupling regime allows for both TZESs and topological MBSs, indicated by red and green arrows in Fig. 5(c), the weak-coupling regime interestingly permits the formation of only MBSs in Fig. 5(d). The robustness and emergence of the TZES for a wide range of parameters at strong coupling is clearly a property that might challenge experimental interpretation. To further illustrate this issue, we plot in color scale in Fig. 5(e) the lowest positive energy level as a function of μ_{sc} and Γ at fixed magnetic field. Here, the TPT is denoted by a dashed green curve, obtained by calculating the Wilson loop in Eq. (3). We have also checked that each point on this curve coincides with the bulk gap closing in our real-space calculations, as it should. The left side of the TPT curve corresponds to the topological phase with E_0 being the energy of the MBSs, while the right side is the trivial phase which hosts TZESs within the region enclosed by the TPT and the dashed red curve. The most relevant feature of this plot is the very large region with TZESs for all larger couplings Γ, which are energywise impossible to distinguish from the phase with MBSs. In contrast, in the weak-coupling regime, TZESs do not even emerge, and this complication is avoided altogether. We have verified that this conclusion also holds in the presence of weak to moderate scalar disorder.

VI. CONCLUSIONS

In this work we have studied the realization of topological superconductivity in a nanowire-superconductor hybrid structure in the presence of an external magnetic field. We have shown that, when the coupling between the nanowire and superconductor is strong, the topological phase transition point is very sensitive to the finite size of the superconductor and, importantly, requires strong magnetic fields to reach the topological phase, a situation that can easily be detrimental to superconductivity. In contrast, in the weak-coupling regime, we have found that the topological transition point is largely insensitive to the finite size of the superconductor and can also be reached by relatively small magnetic fields.

Moreover, very importantly for the practical applicability, the induced energy gap in the topological phase in the weakly coupled regime easily acquires large values similar to those in the strong-coupling regime. This is a result of the induced gap being heavily suppressed in the strong-coupling regime due to both renormalization of the nanowire spin-orbit coupling and the larger magnetic fields needed to reach the topological phase. As a consequence, it is not necessary to use a system with strong coupling between the nanowire and superconductor to achieve a large topological gap, and in fact, the weak-coupling regime is actually more advantageous because it has a large and tunable topological gap, which is of great importance for topological protection of Majorana bound states.

Furthermore, we have also demonstrated that the weak-coupling regime does not allow for the formation of topologically trivial zero-energy states, easily present in strongly coupled superconductor-semiconductor hybrid structures. This stems from the fact that the nanowire chemical potential does not get renormalized in the weak-coupling regime, leading to a homogeneous potential profile in the wire, which cannot accommodate trivial zero-energy states. Our findings thus show clear and multiple advantages of the weak-coupling regime for the realization of low Zeeman field topological superconductivity and Majorana bound states in semiconductor-superconductor hybrid structures.

ACKNOWLEDGMENTS

We acknowledge financial support from the Swedish Research Council (Vetenskapsrådet Grants No. 2018-03488 and No. 2021-04121) and the Knut and Alice Wallenberg Foundation through the Wallenberg Academy Fellows program, as well as the EU-COST Action CA-16218 Nanocohybri. Simulations were enabled by resources provided by the Swedish National Infrastructure for Computing (SNIC) at the Uppsala Multidisciplinary Center for Advanced Computational Science (UPPMAX), partially funded by the Swedish Research Council through Grant No. 2018-05973.

APPENDIX A: BULK SUPERCONDUCTOR

In this Appendix we present further supporting calculations for a thick, or bulklike, SC with $L_y = 41$. In particular, we focus on the low-energy spectrum as a function of the Zeeman field and of the topological transition point as a function of the SC chemical potential to offer direct comparisons with the results in the main text.

1. Phase diagram

In Fig. 6 we present the critical Zeeman field B_c at which the system undergoes a TPT as a function of the chemical potential in the SC $\mu_{\rm sc}$ in the weak, $\Gamma/t_{\rm sc} = 0.2$, 0.3, and strong, $\Gamma/t_{\rm sc} = 0.7$, coupling regimes. This is the same plot as in Fig. 3(b), which instead used a thin SC with $L_y/a = 11$. Here, we clearly observe that $B_{\rm c}$ is considerably larger in the strong-coupling regime and also very dependent on $\mu_{\rm sc}$. In contrast, $B_{\rm c}$ is overall lower and also almost independent of $\mu_{\rm sc}$ in the weak-coupling regime. These findings for thick SCs are in excellent qualitative agreement with the results presented in the main text for thin SCs. As a consequence, the weak-coupling regime allows us to use low Zeeman fields, largely independent of $\mu_{\rm S}$, to reach the topological phase, independent of the size of the SC.

2. Low-energy spectrum and induced gap

In Fig. 7 we show the low-energy spectrum as a function of magnetic field and extracted induced gap as a function of the SC chemical potential, just as in Fig. 4 in the main text but now for a bulk SC. Besides some very slight and irrelevant modifications, the results remain qualitatively the same. In particular, the size of the induced gap is very similar in the weakly and strongly coupled regimes once we enter the topological phase.

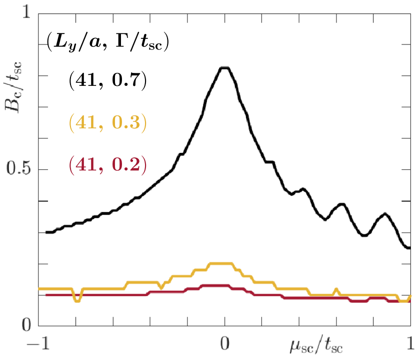

FIG. 6. Same as Fig. 3(b) in the main text, but for $L_y = 41a$.

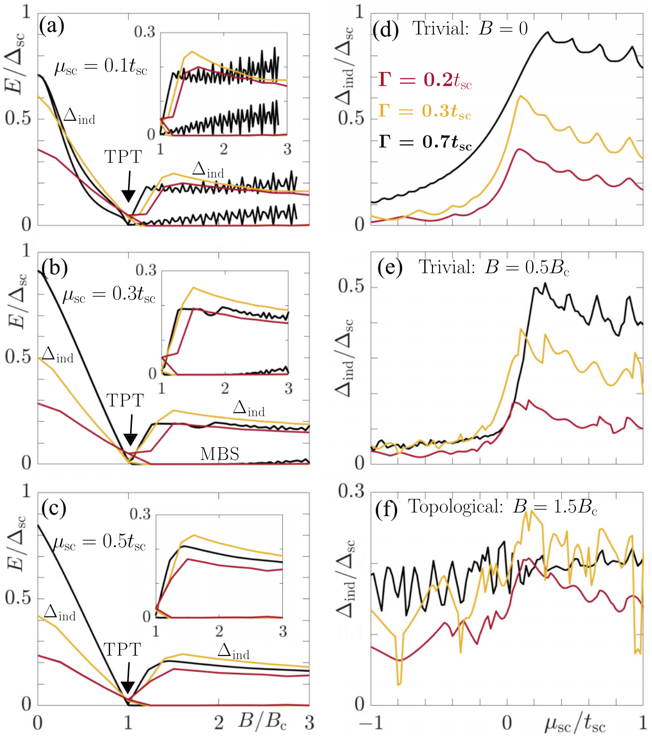

FIG. 7. Same as Fig. 4 in the main text, but for $L_y/a = 41$.

APPENDIX B: LEAKAGE OF LOW-ENERGY STATES INTO SUPERCONDUCTOR

In this Appendix we consider the geometry depicted in Fig. 1(a) and explore how the coupling Γ between the NW and SC influences where in space the lowest-energy wave function Ψ_0 is located. Ideally, the MBSs emerging in the topological regime are situated at the end points of the NW. However, with a finite coupling between the NW and SC, the MBSs can experience a nonvanishing weight also in the SC. In particular, this leakage into the SC might be dependent on the coupling Γ between the NW and SC. To characterize this effect, we therefore calculate the weight of the lowest state in the NW

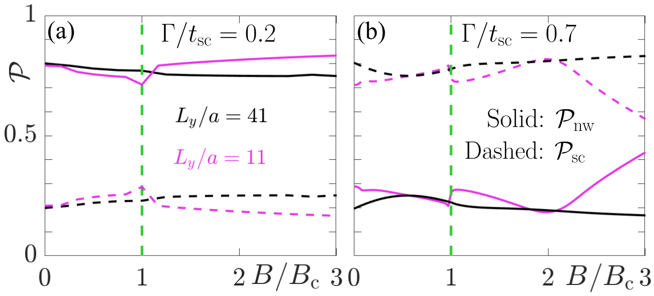

FIG. 8. Weight of the lowest-energy state Ψ_0, $\mathcal{P}$, as a function of Zeeman field $B/B_{\rm sc}$ in the SC (dashed lines) and NW (solid lines) for (a) weak and (b) strong coupling. The green dashed line denotes the TPT. The state for $L_y/a = 11$ is the same state as that given as E_0 in Fig. 4(c) in the main text, while that for $L_y/a = 41$ is the same as that in Fig. 7(c).

and SC as

$$\mathcal{P}_{\rm nw} = \sum_{x=1}^{L_{\rm nw}} |\Psi_{\rm nw}(x)|^2, \quad \mathcal{P}_{\rm sc} = \sum_{i_x=1}^{L_x} \sum_{i_y=1}^{L_y} |\Psi_{\rm sc}(i_x, i_y)|^2, \quad \text{(B1)}$$

where $\mathcal{P} = \sum_{\boldsymbol{r}} |\Psi_0(\boldsymbol{r})|^2 = \mathcal{P}_{\rm nw} + \mathcal{P}_{\rm sc} = 1$ is the wave function probability of the lowest-energy state Ψ_0, with $\mathcal{P}_{\rm nw}$ ($\mathcal{P}_{\rm sc}$) being the fraction or weight of Ψ_0 residing in the NW (SC). We have here also verified that $\mathcal{P} = 1$ for all parameters, as expected for the total probability. However, the individual weights, $\mathcal{P}_{\rm nw}$ and $\mathcal{P}_{\rm sc}$, exhibit distinct behaviors, as seen in Fig. 8, where we present them as a function of the Zeeman field for both thin and thick SCs in the weak [Fig. 8(a)] and strong [Fig. 8(b)] coupling regimes. In the weak-coupling case, the lowest-energy state Ψ_0 resides mainly in the NW for all values of the Zeeman field; that is, both the finite-energy state in the trivial regime and the MBS in the topological regime sit mainly in the NW. The opposite is true for strong coupling; then the lowest-energy state mainly resides in the SC, including the MBS formed in the topological regime. At very large Zeeman fields, Ψ_0 can become equally shared between the SC and NW for thin SCs but not bulk SCs. The detection of MBSs in strongly coupled NW-SC hybrid structures can therefore be difficult as the MBS cannot be fully captured if one probes only the NW. The same problem does not exist in the weakly coupled regime.

[1] A. Kitaev, Periodic table for topological insulators and superconductors, in *Advances in Theoretical Physics: Landau Memorial Conference*, AIP Conf. Proc. No. 1134 (AIP, Melville, NY, 2009), p. 22.

[2] C. Nayak, S. H. Simon, A. Stern, M. Freedman, and S. Das Sarma, Non-Abelian anyons and topological quantum computation, Rev. Mod. Phys. **80**, 1083 (2008).

[3] M. Leijnse and K. Flensberg, Introduction to topological superconductivity and Majorana fermions, Semicond. Sci. Technol. **27**, 124003 (2012).

[4] R. Aguado, Majorana quasiparticles in condensed matter, Riv. Nuovo Cimento **40**, 523 (2017).

[5] R. M. Lutchyn, E. P. A. M. Bakkers, L. P. Kouwenhoven, P. Krogstrup, C. M. Marcus, and Y. Oreg, Majorana zero modes in superconductor-semiconductor heterostructures, Nat. Rev. Mater. **3**, 52 (2018).

[6] H. Zhang, D. E. Liu, M. Wimmer, and L. P. Kouwenhoven, Next steps of quantum transport in Majorana nanowire devices, Nat. Commun. **10**, 5128 (2019).

[7] C. W. J. Beenakker, Search for non-Abelian Majorana braiding statistics in superconductors, SciPost Phys. Lect. Notes 15 (2020).

[8] Y. Oreg and F. von Oppen, Majorana zero modes in networks of Cooper-pair boxes: Topologically ordered states and topological quantum computation, Annu. Rev. Condens. Matter Phys. **11**, 397 (2020).

[9] R. Aguado, A perspective on semiconductor-based superconducting qubits, Appl. Phys. Lett. **117**, 240501 (2020).

[10] R. M. Lutchyn, J. D. Sau, and S. Das Sarma, Majorana Fermions and a Topological Phase Transition in Semiconductor-Superconductor Heterostructures, Phys. Rev. Lett. **105**, 077001 (2010).

[11] Y. Oreg, G. Refael, and F. von Oppen, Helical Liquids and Majorana Bound States in Quantum Wires, Phys. Rev. Lett. **105**, 177002 (2010).

[12] J. Alicea, Majorana fermions in a tunable semiconductor device, Phys. Rev. B **81**, 125318 (2010).

[13] C. J. Bolech and E. Demler, Observing Majorana Bound States in *p*-Wave Superconductors using Noise Measurements in Tunneling Experiments, Phys. Rev. Lett. **98**, 237002 (2007).

[14] K. T. Law, P. A. Lee, and T. K. Ng, Majorana Fermion Induced Resonant Andreev Reflection, Phys. Rev. Lett. **103**, 237001 (2009).

[15] K. Flensberg, Tunneling characteristics of a chain of Majorana bound states, Phys. Rev. B **82**, 180516(R) (2010).

[16] V. Mourik, K. Zuo, S. Frolov, S. Plissard, E. Bakkers, and L. Kouwenhoven, Signatures of Majorana fermions in hybrid superconductor-semiconductor nanowire devices, Science **336**, 1003 (2012).

[17] A. P. Higginbotham, S. M. Albrecht, G. Kirsanskas, W. Chang, F. Kuemmeth, P. Krogstrup, T. S. J. J. Nygård, K. Flensberg, and C. M. Marcus, Parity lifetime of bound states in a proximitized semiconductor nanowire, Nat. Phys. **11**, 1017 (2015).

[18] M. T. Deng, S. Vaitiekėnas, E. B. Hansen, J. Danon, M. Leijnse, K. Flensberg, J. Nygård, P. Krogstrup, and C. M. Marcus, Majorana bound state in a coupled quantum-dot hybrid-nanowire system, Science **354**, 1557 (2016).

[19] S. M. Albrecht, A. P. Higginbotham, M. Madsen, F. Kuemmeth, T. S. Jespersen, J. Nygård, P. Krogstrup, and C. M. Marcus, Exponential protection of zero modes in Majorana islands, Nature (London) **531**, 206 (2016).

[20] H. Zhang, Ö. Gül, S. Conesa-Boj, K. Zuo, V. Mourik, F. K. de Vries, J. van Veen, D. J. van Woerkom, M. P. Nowak, M. Wimmer, D. Car, S. Plissard, E. P. A. M. Bakkers, M. Quintero-Pérez, S. Goswami, K. Watanabe, T. Taniguchi, and L. P. Kouwenhoven, Ballistic superconductivity in semiconductor nanowires, Nat. Commun. **8**, 16025 (2017).

[21] H. J. Suominen, M. Kjaergaard, A. R. Hamilton, J. Shabani, C. J. Palmstrøm, C. M. Marcus, and F. Nichele, Zero-Energy Modes from Coalescing Andreev States in a Two-Dimensional Semiconductor-Superconductor Hybrid Platform, Phys. Rev. Lett. **119**, 176805 (2017).

[22] F. Nichele, A. C. C. Drachmann, A. M. Whiticar, E. C. T. O'Farrell, H. J. Suominen, A. Fornieri, T. Wang, G. C. Gardner, C. Thomas, A. T. Hatke, P. Krogstrup, M. J. Manfra, K. Flensberg, and C. M. Marcus, Scaling of Majorana Zero-Bias Conductance Peaks, Phys. Rev. Lett. **119**, 136803 (2017).

[23] O. Gül, H. Zhang, J. D. S. Bommer, M. W. A. de Moor, D. Car, S. R. Plissard, E. P. A. M. Bakkers, A. Geresdi, K. Watanabe, T. Taniguchi, and L. P. Kouwenhoven, Ballistic Majorana nanowire devices, Nat. Nanotechnol. **13**, 192 (2018).

[24] G. Kells, D. Meidan, and P. W. Brouwer, Near-zero-energy end states in topologically trivial spin-orbit coupled superconducting nanowires with a smooth confinement, Phys. Rev. B **86**, 100503(R) (2012).

[25] E. Prada, P. San-Jose, and R. Aguado, Transport spectroscopy of NS nanowire junctions with Majorana fermions, Phys. Rev. B **86**, 180503(R) (2012).

[26] J. Cayao, E. Prada, P. San-Jose, and R. Aguado, SNS junctions in nanowires with spin-orbit coupling: Role of confinement and helicity on the subgap spectrum, Phys. Rev. B **91**, 024514 (2015).

[27] P. San-José, J. Cayao, E. Prada, and R. Aguado, Majorana bound states from exceptional points in non-topological superconductors, Sci. Rep. **6**, 21427 (2016).

[28] C.-X. Liu, J. D. Sau, T. D. Stanescu, and S. Das Sarma, Andreev bound states versus Majorana bound states in quantum dot-nanowire-superconductor hybrid structures: Trivial versus topological zero-bias conductance peaks, Phys. Rev. B **96**, 075161 (2017).

[29] A. Ptok, A. Kobiałka, and T. Domański, Controlling the bound states in a quantum-dot hybrid nanowire, Phys. Rev. B **96**, 195430 (2017).

[30] C. Fleckenstein, F. Domínguez, N. Traverso Ziani, and B. Trauzettel, Decaying spectral oscillations in a Majorana wire with finite coherence length, Phys. Rev. B **97**, 155425 (2018).

[31] C. Reeg, O. Dmytruk, D. Chevallier, D. Loss, and J. Klinovaja, Zero-energy Andreev bound states from quantum dots in proximitized Rashba nanowires, Phys. Rev. B **98**, 245407 (2018).

[32] M. Hell, K. Flensberg, and M. Leijnse, Distinguishing Majorana bound states from localized Andreev bound states by interferometry, Phys. Rev. B **97**, 161401(R) (2018).

[33] J. Chen, B. D. Woods, P. Yu, M. Hocevar, D. Car, S. R. Plissard, E. P. A. M. Bakkers, T. D. Stanescu, and S. M. Frolov, Ubiquitous Non-Majorana Zero-Bias Conductance Peaks in Nanowire Devices, Phys. Rev. Lett. **123**, 107703 (2019).

[34] T. D. Stanescu and S. Tewari, Robust low-energy Andreev bound states in semiconductor-superconductor structures: Importance of partial separation of component Majorana bound states, Phys. Rev. B **100**, 155429 (2019).

[35] T. Dvir, M. Aprili, C. H. L. Quay, and H. Steinberg, Zeeman Tunability of Andreev Bound States in van der Waals Tunnel Barriers, Phys. Rev. Lett. **123**, 217003 (2019).

[36] A. Vuik, B. Nijholt, A. R. Akhmerov, and M. Wimmer, Reproducing topological properties with quasi-Majorana states, SciPost Phys. **7**, 061 (2019).

[37] J. Avila, F. Peñaranda, E. Prada, P. San-Jose, and R. Aguado, Non-Hermitian topology as a unifying framework for the Andreev versus Majorana states controversy, Commun. Phys. **2**, 133 (2019).

[38] H. Pan and S. Das Sarma, Physical mechanisms for zero-bias conductance peaks in Majorana nanowires, Phys. Rev. Research **2**, 013377 (2020).

[39] C. Jünger, R. Delagrange, D. Chevallier, S. Lehmann, K. A. Dick, C. Thelander, J. Klinovaja, D. Loss, A. Baumgartner, and C. Schönenberger, Magnetic-Field-Independent Subgap States in Hybrid Rashba Nanowires, Phys. Rev. Lett. **125**, 017701 (2020).

[40] D. Razmadze, E. C. T. O'Farrell, P. Krogstrup, and C. M. Marcus, Quantum Dot Parity Effects in Trivial and Topological Josephson Junctions, Phys. Rev. Lett. **125**, 116803 (2020).

[41] O. Dmytruk, D. Loss, and J. Klinovaja, Pinning of Andreev bound states to zero energy in two-dimensional superconductor-semiconductor Rashba heterostructures, Phys. Rev. B **102**, 245431 (2020).

[42] P. Yu, J. Chen, M. Gomanko, G. Badawy, E. P. A. M. Bakkers, K. Zuo, V. Mourik, and S. M. Frolov, Non-Majorana states yield nearly quantized conductance in superconductor-semiconductor nanowire devices, Nat. Phys. **17**, 482 (2021).

[43] M. Valentini, F. Peñaranda, A. Hofmann, M. Brauns, R. Hauschild, P. Krogstrup, P. San-Jose, E. Prada, R. Aguado, and G. Katsaros, Nontopological zero-bias peaks in full-shell nanowires induced by flux-tunable Andreev states, Science **373**, 82 (2021).

[44] E. Prada, P. San-Jose, M. W. de Moor, A. Geresdi, E. J. Lee, J. Klinovaja, D. Loss, J. Nygård, R. Aguado, and L. P. Kouwenhoven, From Andreev to Majorana bound states in hybrid superconductor–semiconductor nanowires, Nat. Rev. Phys. **2**, 575 (2020).

[45] J. Schulenborg and K. Flensberg, Absence of supercurrent sign reversal in a topological junction with a quantum dot, Phys. Rev. B **101**, 014512 (2020).

[46] J. Cayao and P. Burset, Confinement-induced zero-bias peaks in conventional superconductor hybrids, Phys. Rev. B **104**, 134507 (2021).

[47] J. Cayao and A. M. Black-Schaffer, Distinguishing trivial and topological zero-energy states in long nanowire junctions, Phys. Rev. B **104**, L020501 (2021).

[48] P. Marra and A. Nigro, Majorana/Andreev crossover and the fate of the topological phase transition in inhomogeneous nanowires, J. Phys.: Condens. Matter **34**, 124001 (2022).

[49] G.-H. Feng and H.-H. Zhang, Probing robust Majorana signatures by crossed Andreev reflection with a quantum dot, Phys. Rev. B **105**, 035148 (2022).

[50] A. Schuray, D. Frombach, S. Park, and P. Recher, Transport signatures of Majorana bound states in superconducting hybrid structures, Eur. Phys. J.: Spec. Top. **229**, 593 (2020).

[51] G. Zhang and C. Spånslätt, Distinguishing between topological and quasi-Majorana zero modes with a dissipative resonant level, Phys. Rev. B **102**, 045111 (2020).

[52] A. Grabsch, Y. Cheipesh, and C. W. J. Beenakker, Dynamical signatures of ground-state degeneracy to discriminate against Andreev levels in a Majorana fusion experiment, Adv. Quantum Technol. **3**, 1900110 (2020).

[53] Y. Zhang, K. Guo, and J. Liu, Transport characterization of topological superconductivity in a planar Josephson junction, Phys. Rev. B **102**, 245403 (2020).

[54] A. Mukhopadhyay and S. Das, Thermal signature of the Majorana fermion in a Josephson junction, Phys. Rev. B **103**, 144502 (2021).

[55] H. Zhang, M. W. A. de Moor, J. D. S. Bommer, D. Xu, G. Wang, N. van Loo, C.-X. Liu, S. Gazibegovic, J. A. Logan, D. Car, R. L. M. Op het Veld, P. J. van Veldhoven, S. Koelling, M. A. Verheijen, M. Pendharkar, D. J. Pennachio, B. Shojaei, J. S. Lee, C. J. Palmstrøm, E. P. A. M. Bakkers, S. D. Sarma, and L. P. Kouwenhoven, Large zero-bias peaks in InSb-Al hybrid semiconductor-superconductor nanowire devices, arXiv:2101.11456 (2021).

[56] S. Das Sarma and H. Pan, Disorder-induced zero-bias peaks in Majorana nanowires, Phys. Rev. B **103**, 195158 (2021).

[57] C. Reeg, D. Loss, and J. Klinovaja, Metallization of a Rashba wire by a superconducting layer in the strong-proximity regime, Phys. Rev. B **97**, 165425 (2018).

[58] C. Reeg, D. Loss, and J. Klinovaja, Proximity effect in a two-dimensional electron gas coupled to a thin

superconducting layer, Beilstein J. Nanotechnol. **9**, 1263 (2018).

[59] O. A. Awoga, J. Cayao, and A. M. Black-Schaffer, Supercurrent Detection of Topologically Trivial Zero-Energy States in Nanowire Junctions, Phys. Rev. Lett. **123**, 117001 (2019).

[60] A. C. Potter and P. A. Lee, Engineering a $p+ip$ superconductor: Comparison of topological insulator and Rashba spin-orbit-coupled materials, Phys. Rev. B **83**, 184520 (2011).

[61] T. D. Stanescu, R. M. Lutchyn, and S. Das Sarma, Majorana fermions in semiconductor nanowires, Phys. Rev. B **84**, 144522 (2011).

[62] D. Chevallier, P. Simon, and C. Bena, From Andreev bound states to Majorana fermions in topological wires on superconducting substrates: A story of mutation, Phys. Rev. B **88**, 165401 (2013).

[63] T. D. Stanescu and S. Tewari, Majorana fermions in semiconductor nanowires: Fundamentals, modeling, and experiment, J. Phys.: Condens. Matter **25**, 233201 (2013).

[64] W. S. Cole, S. Das Sarma, and T. D. Stanescu, Effects of large induced superconducting gap on semiconductor Majorana nanowires, Phys. Rev. B **92**, 174511 (2015).

[65] T. D. Stanescu and S. Das Sarma, Proximity-induced low-energy renormalization in hybrid semiconductor-superconductor Majorana structures, Phys. Rev. B **96**, 014510 (2017).

[66] C. Reeg, D. Loss, and J. Klinovaja, Finite-size effects in a nanowire strongly coupled to a thin superconducting shell, Phys. Rev. B **96**, 125426 (2017).

[67] M. W. A. de Moor, J. D. S. Bommer, D. Xu, G. W. Winkler, A. E. Antipov, A. Bargerbos, G. Wang, N. van Loo, R. L. M. O. het Veld, S. Gazibegovic, D. Car, J. A. Logan, M. Pendharkar, J. S. Lee, E. P. A. M. Bakkers, C. J. Palmstrøm, R. M. Lutchyn, L. P. Kouwenhoven, and H. Zhang, Electric field tunable superconductor-semiconductor coupling in Majorana nanowires, New J. Phys. **20**, 103049 (2018).

[68] P.-G. de Gennes, *Superconductivity of Metals and Alloys* (Westview, FL, Boulder, Colorado, 1999)

[69] W. E. Arnoldi, The principle of minimized iterations in the solution of the matrix eigenvalue problem, Q. Appl. Math. **9**, 17 (1951).

[70] O. A. Awoga, K. Björnson, and A. M. Black-Schaffer, Disorder robustness and protection of Majorana bound states in ferromagnetic chains on conventional superconductors, Phys. Rev. B **95**, 184511 (2017).

[71] A. Theiler, K. Björnson, and A. M. Black-Schaffer, Majorana bound state localization and energy oscillations for magnetic impurity chains on conventional superconductors, Phys. Rev. B **100**, 214504 (2019).

[72] M. Mashkoori and A. Black-Schaffer, Majorana bound states in magnetic impurity chains: Effects of d-wave pairing, Phys. Rev. B **99**, 024505 (2019).

[73] A. Alexandradinata, X. Dai, and B. A. Bernevig, Wilson-loop characterization of inversion-symmetric topological insulators, Phys. Rev. B **89**, 155114 (2014).

[74] A. Bouhon and A. M. Black-Schaffer, Global band topology of simple and double Dirac-point semimetals, Phys. Rev. B **95**, 241101(R) (2017).

[75] M. Mashkoori, S. Pradhan, K. Björnson, J. Fransson, and A. M. Black-Schaffer, Identification of topological superconductivity in magnetic impurity systems using bulk spin polarization, Phys. Rev. B **102**, 104501 (2020).

[76] A. Kobiałka, N. Sedlmayr, and A. Ptok, Majorana bound states in a superconducting Rashba nanowire in the presence of antiferromagnetic order, Phys. Rev. B **103**, 125110 (2021).

[77] A. Maiani, R. Seoane Souto, M. Leijnse, and K. Flensberg, Topological superconductivity in semiconductor-superconductor-magnetic-insulator heterostructures, Phys. Rev. B **103**, 104508 (2021).

[78] D. Rainis and D. Loss, Majorana qubit decoherence by quasiparticle poisoning, Phys. Rev. B **85**, 174533 (2012).

[79] J. Alicea, New directions in the pursuit of Majorana fermions in solid state systems, Rep. Prog. Phys. **75**, 076501 (2012).